Nanostructured Triblock Copolymers with Chemically Complementary Components and Their Ionic Conductivity

Tatyana Zheltonozhskaya[1,*], Elena Shembel[2], Sergey Fedorchuk[1], Larisa Kunitskaya[1], Iryna Maksyuta[2], Nataliya Permyakova[1] and Yuriy Gomza[3]

[1]*Kiev National Taras Shevchenko University, Faculty of Chemistry, Department of Macromolecular Chemistry, 60 Vladimirskaya St., 01033 Kiev, Ukraine*

[2]*Ukrainian State Chemical-Engeneering University, Laboratory of Electrochemical Current Sources, 8 Gagarin St., 49005 Dnipropetrovsk, Ukraine*

[3]*Institute for Macromolecular Chemistry, National Academy of Sciences of Ukraine, 48 Kharkovskoye Shosse, 02160 Kiev, Ukraine*

Abstract: A series of structural and electrochemical studies of the triblock copolymers (TBCs) based on poly(ethylene oxide) (M_n = 14 and 35 kDa) and polyacrylamide (PAAm-*b*-PEO-*b*-PAAm), which formed the intramolecular polycomplexes, were carried out using nuclear magnetic resonance, differential scanning calorimetry, wide-angle and small-angle X-ray scattering, and impedance spectroscopy. The combination of the amorphous mass-fractal-organized structure of the copolymers with high level of the ionic conductivity of pure TBCs and their compositions with the couple KI/I_2 and $LiPF_6$ salt was established. Possible reasons for the effects in the context of applications of TBC compositions in solar cells and lithium batteries are discussed.

Keywords: Block copolymer, structure, intramolecular polycomplex, ionic conductivity, electrochemical devices.

1. INTRODUCTION

The poly(ethylene oxide) (PEO)-based solid polymer electrolytes have many potential applications in different electrochemical devices such as dye-sensitized solar cells (DSSCs), solid-state lithium batteries (SSLB) and organic solar cells [1-11]. In DSSCs, a solid polymer electrolyte would provide not only a high ionic conductivity between the photoelectrode, which comprises the dye-attached nanoscale metal oxide (in particular, titanium dioxide), and the counter electrode with platinum catalyst layer but also a large interfacial contact area between the electrolyte and dye, thus enhancing the efficacy of the light energy transformation [12-14].

Crystallization of PEO sharply reduces the mobility of its segments and decreases the conductivity of polymeric matrix. Therefore, numerous efforts were done to find the ways to increase the ionic conductivity of the PEO-containing electrolytes and simultaneously to lower or even to prevent the crystallization phenomenon. The following operations were carried out for this purpose: i) the alkali metal salts with the large volume of counter ions (perchlorate, tetrafluoroborate, bis[perfluoro(alkylen)sulfonyl] imide and other anions) were introduced in the content of solid polymeric electrolytes [3,15-17]; ii) terminal groups of PEO chains were modified [12,18]; iii) other co-monomers were introduced into PEO chains [4,5]; iv) the PEO-containing solid-state electrolytes were additionally filled with amorphous oligomers [6], other polymers [19-22], different nanoparticles [5,23-25] or nanotubes [26-28] and plasticizers [11,29]; v) the block and graft copolymers comprised PEO and amorphous components such as poly(propylene oxide), polystyrene, poly[alkyl(meth)acrylates] etc. were created and used as matrices in solid electrolytes [30-33]; vi) PEO chains were cross-linked [34-36].

In the case of linear block copolymers, the largest decrease in the crystallinity degree of PEO, X_c, was observed in the triblock copolymers with PEO central block and two side amorphous blocks [37]. When the length of side amorphous blocks became higher than a certain critical value, which depended on chemical nature of the blocks and PEO length, the triblock copolymers completely lost their capability of crystallization [38]. In the graft copolymers contained PEO grafts, X_c value was the lower, the less the length and quantity (density) of grafted chains. The relationship between X_c and the parameters pointed was opposite in the graft copolymers, where PEO was the main chain [30].

There is also one more way to produce solid-state polymer electrolytes with practically full suppression of

*Address corresponding to this author at the Department of Macromolecular Chemistry, Kiev National Taras Shevchenko University, Faculty of Chemistry, 60 Vladimirskaya St., 01033 Kiev, Ukraine; Tel: +38 (044) 2393411; Fax: +38 (044) 2393100; E-mail: zheltonozhskaya@ukr.net

E-ISSN: 1929-5995/12

PEO crystallization, namely, application as polymeric matrices the intermolecular polycomplexes (InterPCs), which are formed between PEO and polyacids or other proton-donor polymers by means of hydrogen bonds [39-41]. Indeed, the amorphous bulk structure of such InterPCs and their enhanced binding capability with respect to different ions, organic substances and colloidal particles are well known [42,43]. At the same time, the main drawback of InterPCs such as potential capability of disintegration to separate components under the effect of external stimuli (temperature, pH and so on) and/or strong competitors (solvent molecules, ions and other additives), which destroy an initial H-bond system, is well known too [44]. This can negatively influences the formation and exploitation of multicomponent polymer electrolytes based on InterPCs.

We consider that the application of the PEO-containing intramolecular polycomplexes (IntraPCs) [45] as polymeric matrices is essentially more perspective. These IntraPCs are formed in macromolecules of the double hydrophilic block and graft copolymers with chemically complementary components and combine properties of both the block-type copolymers and InterPCs. Interacting components are additionally fixed in IntraPCs by covalent bond(s); due to this they can demonstrate higher stability in many competitive processes, which accompany the formation of multicomponent polymer electrolytes. Moreover, IntraPCs possess by high binding capability as InterPCs [45]. The interest to the PEO-containing IntraPCs sharply increased last decade [45,46] but their ionic conductivity was not practically investigated in the interrelationship with a bulk structure.

In the present work, we studied the ionic conductivity of PAAm-b-PEO-b-PAAm triblock copolymers (TBCs), which contained amorphous polyacrylamide and formed IntraPCs, and also multicomponent systems comprised TBCs. It was shown earlier [47] that due to existence of both the long amorphous chains of PAAm and IntraPC formation, TBC structure preserved an amorphous character also at a high length of PEO block (up to M_n ~ 40 kDa). This fact and also well-known capability of PEO oxygen atoms [1,3] and PAAm amide groups [48] to connect different ions were dominant for a production of solid-state electrolytes based on pure TBC films and those doped by ionic components. The electrolyte for DSSCs was doped by the Red/Ox couple KI/I_2, which is usually applied for a regeneration of the oxidized dye [6,10,13,14], unlike the electrolyte for SSLB, which was filled with lithium salt ($LiPF_6$).

2. EXPERIMENTAL SECTION

2.1. (Co)Polymer Syntheses

In TBC syntheses, poly(ethylene glycol) with M_n = 14 (PEG1) and 35 kDa (PEG2) and cerium ammonium nitrate from “Aldrich” (USA) and also acrylamide (AAm) from “Merck” (Germany) were used. The monomer was twice re-crystallized from chloroform before a synthesis. All syntheses were carried out in the deionized water using a template radical block copolymerization, in which PEO radicals formed by Red/Ox reaction between terminal hydroxyl groups of PEG and Ce^{IV} ions participated [45]. The molar ratio of $[Ce^{IV}]/[PEG]$ = 2 and the monomer concentration of [AAm] = 1 mol·dm^{-3} were applied. The reaction blend was mixed in an inert atmosphere at 20 °C for 24 h. Homopolymerization of AA was carried out in analogous conditions using ethanol instead PEG to initiate a radical process. The synthesized samples of TBC1-TBC3 and PAAm were re-precipitated by acetone, dissolved again in the deionized water and freeze dried. Final dried polymer samples had a porous structure, due to this they resembled a wadding.

2.2. Molecular Structure Characterization

In order to confirm the chemical structure of TBCs and to determine the molecular weights of PAAm blocks and TBC macromolecules, the nuclear magnetic resonance (NMR) spectroscopy was applied. ^{1}H NMR spectra were recorded in the deuterated water (C = 10 kg·m^{-3}) at 400 MHz and 20 ºC using a Mercury-400 instrument from “Varian” (USA). The chemical shifts, δ, were determined relatively to tetramethylsilane as a standard. Molecular parameters of PAAm (M_w = 81 kDa, M_w/M_n = 1.38) were found by gel permission chromatography.

2.3. Differential Scanning Calorimetry (DSC)

The bulk structure of TBCs was characterized first by DSC using a DSC-910 microcalorimeter and “Du Pont”-1090 (USA) thermoanalyzer. To determine parameters of structural transitions, the instrument was calibrated by indium and zinc. Moreover, the crystal of a sapphire was heated together with the copolymers to calculate the temperature dependences of the specific heat capacity, C_p, basing on the heat flow curves. Polymer samples (~ 10 mg) were carefully dried in a vacuum case and vacuum-desiccator above $CaCl_2$.

Then the samples were placed in the opened DSC pans, cooled by liquid nitrogen, and heated with a rate of 16 °C·min^{-1}.

2.4. Wide-Angle X-Ray Scattering (WAXS)

WAXS profiles of TBC films were obtained using a DRON-2.0 X-ray difractometer. The copolymer films were cast from aqueous solutions on the Teflon surface and dried in a vacuum case for one week. They had a homogeneous glassy structure. The film piles with a thickness of ~ 1 mm were used in the experiments. The monochromatic Cu-K_α radiation with λ = 0.154 nm, filtered by Ni, was provided by an IRIS-M7 generator at an operating voltage of 30 kV and a current of 30 mA. The scattering intensities were measured by a scintillation detector, scanning in 0.2° steps over the range of the θ = 3-40° scattering angles (respectively q = 2.13-31.21 nm^{-1}, where $q = 4\pi\cdot\sin(\theta/2)/\lambda$ is the wavevector or the scattering vector). The diffraction curves obtained were reduced to equal intensities of the primary beam and equal values of the scattering volume [49]. Also, the normalization of experimental scattering intensities was carried out according to the (1) formula:

$$I_{n(i)}(\theta) = [I_{\exp}(\theta) - I_b(\theta)] \cdot (I/I_0), \quad (1)$$

where $I_{exp}(\theta)$ and $I_{n(i)}(\theta)$ are the experimental and normalized intensities in WAXS profile as a function of θ, $I_b(\theta)$ is the intensity of the background for every θ value, I_0 and I are the intensities of incident and scattered beams at θ = 0° (the coefficient of the beam weakening).

2.5. Small-Angle X-Ray Scattering (SAXS)

SAXS experiments were carried out using an automated Kratky slit-collimated camera. Here copper anode emission, which was monochromated by the total internal reflection and nickel filter, was used. The intensity curves were recorded in the step-scanning mode of the scintillation detector in the θ = 0.03-4.0° region, which corresponded to the q = 0.022-2.86 nm^{-1} wavevector region. Thus, the study of micro-scale heterogeneous domains with characteristic dimensions (evaluated as $2\pi/q$) from 2 to 280 nm was possible. Preliminary processing of SAXS profiles was carried out using the FFSAXS-3 program [49] and etalon sample from the laboratory of professor Kratky. The scattering intensities were normalized by the sample thickness and the scattering intensity of an etalon. Additionally, the raw intensity curves were smoothed, corrected for parasitic scattering and desmeared.

2.6. Impedance Spectroscopy

In order to measure the ionic conductivity, the films (~5x5 cm) of pure TBCs and their compositions with the couple KI/I_2 (at a constant molar ratio of 1.83) and $LiPF_6$ salt were cast from aqueous solutions on the Teflon surface and dried on air for 3-4 days. The copolymer films doped with KI/I_2 had a deep brown colour and homogeneous glassy structure; they were also transparent. Unlike this, TBC films filled with $LiPF_6$ had a white colour and were more flexible. The specific ionic conductivity, σ, of the samples was determined by impedance spectroscopy [50]. All the experiments were carried out in a special cell with blocking Pt electrodes in the 0.001-100 kHz frequency range at 20 °C using a Voltalab instrument (USA) with computer program Voltalab Master. The measuring protocols A, B and C were applied. A: a dry film was squeezed between the electrodes in a cell. B: a dry film was squeezed between the electrodes moistened by water; in this case a strong adhesion between electrodes and film took place. C: the initial procedure was analogous to the protocol B but all the measurements were carried out without a cell using the electrodes “stuck” together by a film. The effect of swelling was observed in the films at B and C protocols and resulted in the change of their thickness. In some cases, a nonionic plasticizer ethylene glycol (EG) was introduced in the compositions too.

3. RESULTS AND DISCUSSION

3.1. Chemical Structure and Molecular Parameters of the Copolymers

The examples of ^{1}H NMR spectra for PEG2, PAAm and TBC2 are shown in Figure **1**:

The proton signal of methylene groups, ***a***, with δ = 3.68 ppm was displayed in the spectra of all PEGs. The signals of methine, ***b***, and methylene, ***c***, groups with δ = 1.4-1.8 and 2.1-2.4 ppm, consequently, were observed in the spectrum of PAAm. The spectrum of TBC2 and other copolymers contained all the signals pointed, thus confirming the presence of PEO and PAAm blocks in TBC macromolecules. Using the integral intensities, A, of the signals ***a*** and ***c*** and also the known molecular weights of PEG, the number-average molecular weights of PAAm side blocks in TBCs were calculated according to the (2) formula:

$$M_{n\cdot PAAm} = \frac{2 \cdot M_{0\cdot PAAm} \cdot M_{nPEO} \cdot A_c}{M_{0PEO} \cdot A_a}, \quad (2)$$

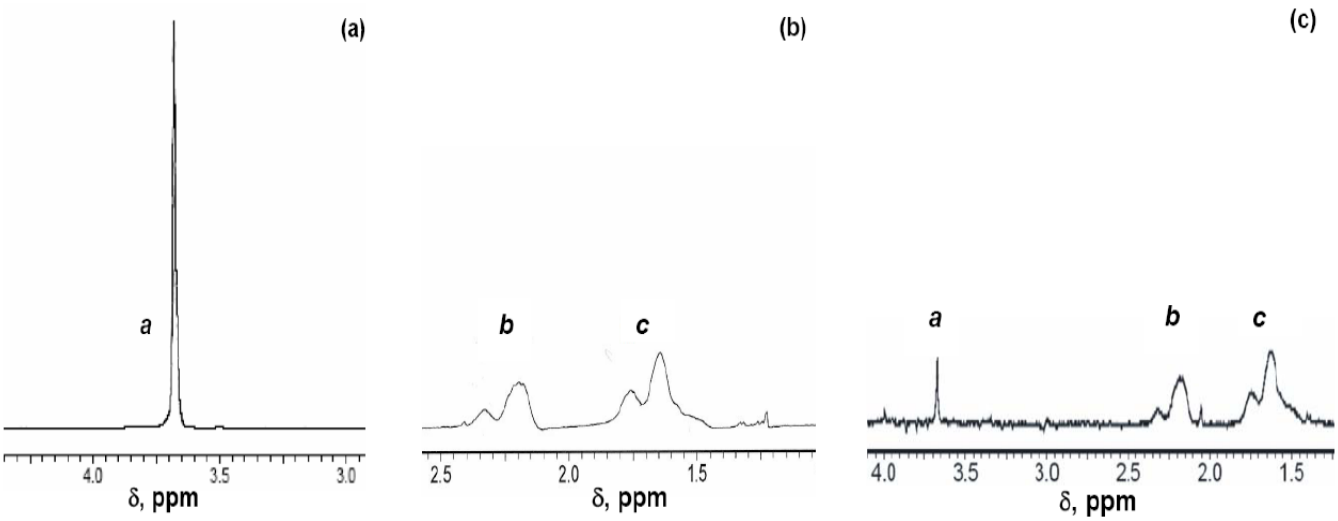

Figure 1: ^{1}H NMR spectra of (**a**) PEG2, (**b**) PAAm, and (**c**) TBC2 in D_2O (C = 10 kg·m^{-3}) at 20 ºC. Designations **a**, **b**, **c** correspond to the signals of methylene protons of PEO and methine and methylene protons of PAAm, consequently.

where $M_{0\ PAAm}$ and $M_{0\ PEO}$ are the molecular weights of PEO and PAAm repeat units. All molecular characteristics of TBCs are collected in Table **1**:

According to the data of Fourier transform infrared spectroscopy (FTIR), which were obtained earlier [51], the system of hydrogen bonds with high thermostability exists in TBCs as between PEO and PAAm blocks (Figure **2**) as between PAAm segments (such as *cis*-*trans*-multimers of amide groups). Obviously, that the interaction of PEO and PAAm blocks would be mainly intramolecular-type (within separate macromolecules of TBCs) in dilute aqueous solutions and intermolecular-type (between different copolymer macromolecules) in the concentrated TBC solutions and their films.

3.2. Morphology of the Copolymer Films

A bulk structure of TBC1 and TBC2 samples was characterized first by DSC method. Corresponding thermograms (the 1-st and 2-nd scans) are shown in Figure **3**. They contained an intense peak of water evaporation near 100 °C and a single glass transition, which parameters are shown in Table **2**. These data indicated a full compatibility of the polymer components and the absence of PEO crystalline regions in TBC

Table 1: Molecular Parameters of the Triblock Copolymers

Copolymer	M_{nPEO}, kDa	M_{nPAAm}, kDa	M_{nTBC}, kDa[a]	w_{PEO}, wt/%[b]
TBC1	14	266	545	2.6
TBC2	35	1095	2225	1.6
TBC3	35	1823	3681	1.0

[a]The molecular weight of the copolymer was calculated by formula: $M_{nTBC} = M_{nPEO} + 2 \cdot M_{nPAAm}$
[b]The weight fraction of PEO block in the copolymer.

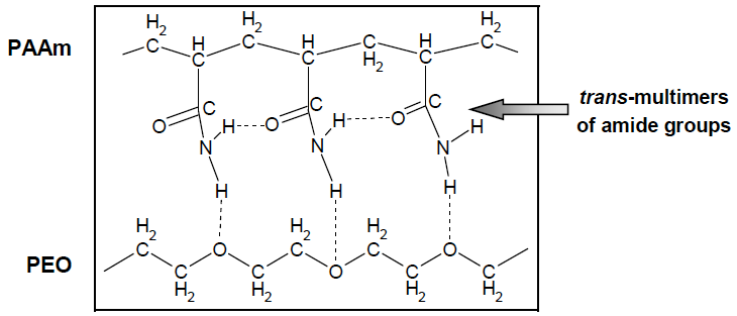

Figure 2: The hydrogen bond system between PEO and PAAm blocks in the copolymers.

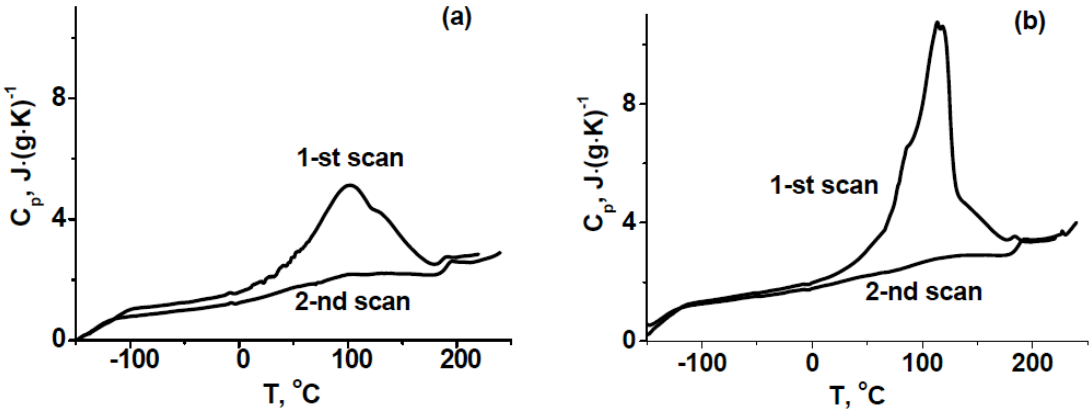

Figure 3: DSC thermograms (the 1-st and 2-nd scans) of (**a**) TBC1 and (**b**) TBC2. The heating rate is 16 °C·min^{-1}.

Table 2: Characteristics of the Glass Transition in the Copolymer Bulk Structure

Copolymer	Scan	T_g, °C[a]	ΔT_g, °C[b]	ΔC_p, J·(g·K)$^{-1}$[c]	T_g*, °C[d]
TBC1	2	188.7	5.4	0.47	186.8
TBC2	2	185.9	5.2	0.57	188.3

[a]The glass transition temperature.
[b]The temperature region for the glass transition.
[c]The specific heat capacity jump.
[d]The glass transition temperature found by the (2) relation for corresponding PEG/PAAm blend.

structure. Therefore, the amorphous structure of TBC1 and TBC2 could be represented as PAAm matrix, where small domains formed by the H-bonded PEO and PAAm segments are distributed.

We used further T_g and ΔC_p values for PEG (T_{g1} = -57 °C and ΔC_{p1} = 0.25 J·(g·K)$^{-1}$ from the study [52]) and PAAm (T_{g2} = 190.9 °C and ΔC_{p2} = 0.55 J·(g·K)$^{-1}$ from the study [48]) and also the weight fractions, w_1 and w_2, for both the components in TBCs from Table **1** in order to carry out the T_g-composition analysis by the Kouchman-Karasz relation (3). Note, that this relation was developed for compatible polymer blends with specific interactions [53]:

$$\ln\left(\frac{T_g^*}{T_{g1}}\right) = \frac{w_2 \cdot \Delta C_{p2} \cdot \ln\left(T_{g2} / T_{g1}\right)}{w_1 \cdot \Delta C_{p1} + w_2 \cdot \Delta C_{p2}} \quad (3)$$

Using the (3) formula, we calculated T_g* values for two PEG/PAAm blends contained the same weight fractions of the components as TBC1 and TBC2 (Table **2**). They turned out to be in a good agreement with T_g numbers, which were experimentally found for both TBC samples (Table **2**). Thus, the conclusion about a high compatibility of the polymeric components in TBC structure was confirmed.

Additional structural properties of TBCs were established by WAXS and SAXS. Corresponding profiles for two TBC samples are shown in Figure **4**. The data for TBC3 sample were analogous. Two diffusive overlapped maxima were observed in WAXS difractograms of TBCs (Figure **4a**). They were assigned to the presence of two systems of planes in the paracrystalline lattice, which characterizes TBC amorphous structure [47]. The first maximum at $\theta \sim 15°$ with smaller intensity reflected the lateral periodicity in the arrangement of PAAm chains. The second one at θ = 22.1° with greater intensity was caused by a periodic arrangement of the flat H-bonded *cis*-dimmers of amide groups in the structures of *cis-trans*-multimers [45,51]. Analogous maxima were also displayed in WAXS difractograms of pure PAAm [47].

A sharp smooth decay in the scattering intensity versus the wavevector (without any peaks or diffusive maxima) was observed in SAXS profiles of TBCs (Figure **4b**) that suggested the absence of any periodicity in the arrangement of separate structural elements of TBCs at the supramolecular level. Due to these results, the homogeneity of TBC structure on different structural levels was fully proved. This meant that the domains contained the hydrogen-bonded PEO and PAAm segments were uniformly distributed within PAAm matrix. But the more important and interesting fact consisted in non-monolithic (nanoporous) character of glassy TBC films. Such conclusion has been achieved by the analysis of SAXS profiles, which

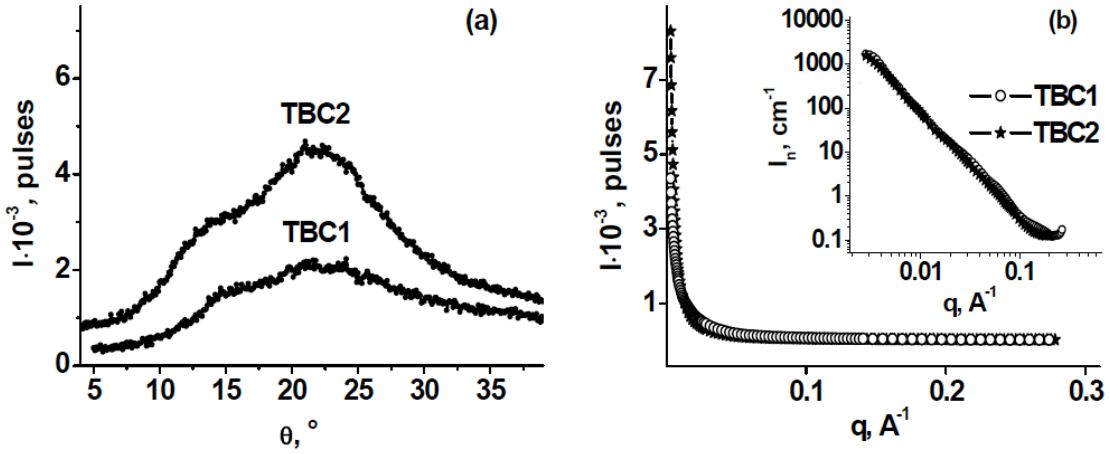

Figure 4: The intensities of (**a**) wide-angle and (**b**) small-angle X-ray scattering for TBC1 and TBC2 samples vs the scattering angle and wavevector consequently. SAXS profiles in the double logarithmic coordinates are shown in figure (**b**) in a lesser scale.

were normalized by the sample thickness and scattering intensity of a standard and then were represented in the double logarithmic coordinates (these plots are shown in Figure **4b** in a lesser scale). The linear decrease in log *I* versus log *q* was observed practically over the whole region of the wavevectors under study and corresponded to the power scattering law by Porod ($I \approx q^{-Df}$) [54,55]. The parameter D_f (the slope tangent of this straight line or the fractal dimension) was equal to 2.4 in the cases of TBC1 and TBC2. Such value ($D_f < 3$) is known to reflect the presence of the porous mass-fractal-organized structure [54-56] in the copolymer films. The mass-fractal clusters (Figure **5**) with the D_f = 2.4 fractal dimension could be considered as separate elements of this structure [54].

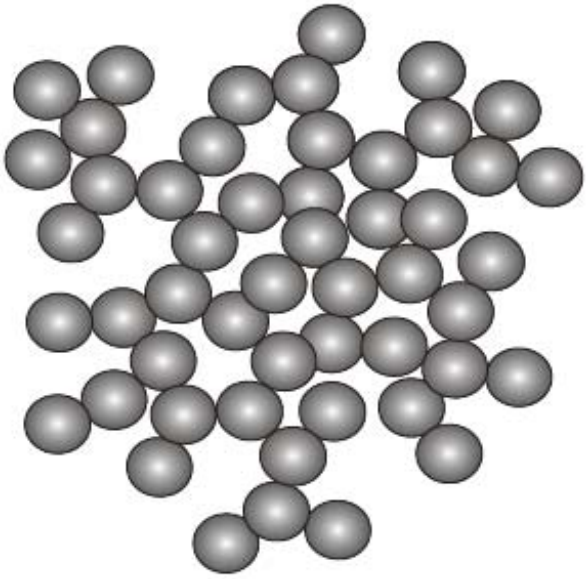

Figure 5: Schematic construction of the branched mass-fractal cluster in TBC amorphous structure.

3.2. Ionic Conductivity

Impedance spectroscopy is widely used to study electrochemical properties of different materials [50,57]. Electrochemical impedance is usually measured by applying a sinusoidal potential excitation to an electrochemical cell and then by measuring the current through the cell [57]. At a small excitation signal, the current response is pseudo-linear and sinusoidal with the same frequency but shifted in time. The complex frequency-dependent resistance or impedance, Z(ω), of some electrochemical cell with Pt electrodes, which are blocking electrode reactions, contains two contributions [50,57]:

$$Z(\omega) = Z_r + jZ_i \; Z_r = R \; Z_i = 1/(\omega \cdot C), \quad (4)$$

where Z_r and jZ_i are consequently the real (resistive) and imaginary (capacitive) parts of the complex impedance, $j = \sqrt{-1}$ is the complex number, R and C are the volume resistance and capacity of the cell, ω is the radial frequency [50]. Due to studying frequency dependences of both the contributions, the determination of the specific ionic conductivity of polymer electrolytes is possible. The impedance spectra of TBC2 and its compositions with the couple KI/I_2, which ones are represented as dependences of the imaginary part of the complex impedance versus the real part (Nyquist Plots [57]), are shown in Figure **6**. Note that each point on the Nyquist Plot is the impedance Z at one frequency.

It can be seen that the entire semicircular portion in the complex impedance representation was absent, led to a conclusion that the total conductivity is mainly the result of ionic conductivity.

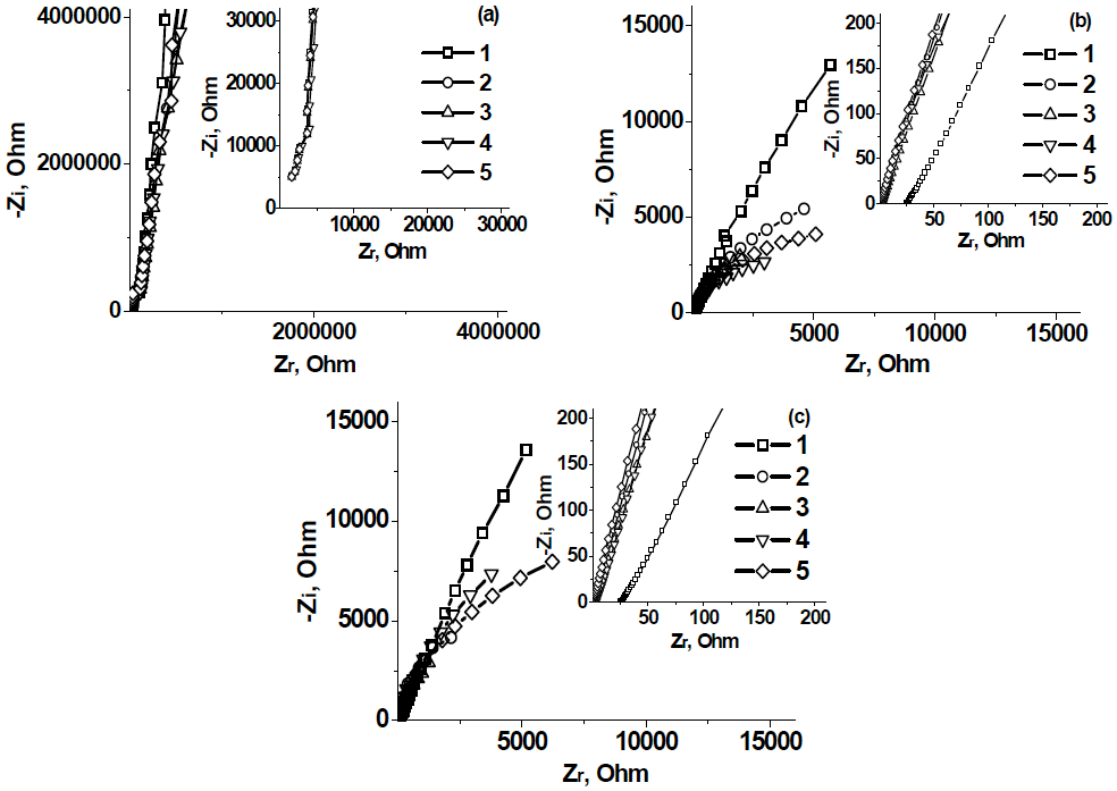

Figure 6: Impedance spectra (the dependences of the imaginary parts Zi of the complex impedance vs the real parts Zr) for a pure TBC2 (film 1 in Table **3**) and its compositions with KI/I_2 (films 2-5), which were measured in the 0.001-100 kHz frequency range using the protocols: (**a**) A, (**b**) B and (**c**) C (see the text). The regions of large frequencies are shown in figures (**a**-**c**) in a lesser scale. The $[KI]/[I_2]$ = 1.83 molar ratio was constant in all the cases.

The volume resistance of the films at the infinitely high frequency was determined by the linear extrapolation of these impedance data to the abscissa-axis. Such extrapolation is typical in the studies of polymer electrolytes [16,58]. The specific ionic conductivity was calculated according to the (3) relation [16]:

$$\sigma = l / (R_{\infty} \cdot S), \quad (3)$$

where l is the film thickness; S is the electrode area; R_{∞} is the volume resistance of a film at the infinitely high frequency.

The results are shown in the right part of Table **3**. Even a dry film of pure TBC2 displayed the high level of the ionic conductivity as compared to the films of: i) a partially cryatalline pure PEO with M_w=600 kDa (σ = $8.35 \cdot 10^{-10}$ [59] or ~$3 \cdot 10^{-10}$ $S \cdot cm^{-1}$ [28] at 25 °C) and ii) an amorphous dry layer-by-layer PEO/PAAc composition (σ = $3.9 \cdot 10^{-11}$ $S \cdot cm^{-1}$ at 25 °C and pH = 2.5) [41]. This effect could be explained by the following. Firstly, both TBC components are highly hydrophilic that results in the presence of ~10 wt/% moisture even in the carefully dried TBC films (the data of dynamic thermogravimetric analysis, DTGA). Actually, every oxygen atom of PEO can adsorb 2 water molecules whereas every amide group of PAAm can connect up to 4 water molecules. Further, PEO chains lose their ability of crystallizing because of the interaction with PAAm chains. Therefore, the mobility of PEO chains keeps and promotes the conductivity growth. Finally, the nanoporous mass-fractal organization of TBC structure ensures a free transport of the ions, which are contained in the adsorbed water and possibly in the copolymer sample after synthesis (see above-mentioned synthetic strategy), throughout the copolymer films under the action of electric field. An important role of the porous film structure in the increase of their ionic conductivity was also noted in the studies [25,60]. Introduction of KI/I_2 caused the regular increase in the film conductivity in 10-24 % that depended on the electrolyte concentration (Table **3**). It should be noted that the achieved ionic conductivity for the dried composite TBC films (σ_{max} = $3.6 \cdot 10^{-6}$ $S \cdot cm^{-1}$ at 20 °C and a ratio of [TBC]/[KI] ≈ 20÷30 base-mol·mol^{-1}) turned out to be higher than that for the analogous composite PEO films (σ_{max} ~ $2 \cdot 10^{-6}$ $S \cdot cm^{-1}$ at 25 °C and the molar ratios: [EO]/[KI] ≈ 24 and $[KI]/[I_2]$ = 9) [61].

Table 3: Ionic Conductivity of a Pure Triblock Copolymer and that Doped by KI/I_2

Film	System	[PEO] / [KI], base-mol·mol^{-1}	[TBC] / [KI], base-mol·mol^{-1}	Method	l,[a] μm	R_∞,[b] Ohm	σ,[c] S·cm^{-1}
1	TBC2	-	-	A	90	2000	$2.9\cdot10^{-6}$
				B	160	26	$4.0\cdot10^{-4}$
				C		27	$3.8\cdot10^{-4}$
2	TBC2+KI/I_2	1.5	59.5	A	100	2000	$3.2\cdot10^{-6}$
				B	130	1	$8.4\cdot10^{-3}$
				C		0.9	$9.4\cdot10^{-3}$
3	TBC2+KI/I_2	0.8	29.6	A	100	1800	$3.6\cdot10^{-6}$
				B	140	1.5	$6.1\cdot10^{-3}$
				C		1.6	$5.7\cdot10^{-3}$
4	TBC2+KI/I_2	0.5	19.7	A	100	2000	$3.6\cdot10^{-6}$
				B	110	1.2	$5.4\cdot10^{-3}$
				C		1.2	$5.4\cdot10^{-3}$
5	TBC2+KI/I_2	0.4	14.8	A	90	2000	$2.9\cdot10^{-6}$
				B	110	0.9	$8.0\cdot10^{-3}$
				C		0.8	$8.9\cdot10^{-3}$

[a]The thickness of a polymer film between the electrodes.
[b]The volume resistance of a polymer film at the infinitely high frequency.
[c]The specific ionic conductivity.

At the same time, the highest effects were observed at a film testing in the regimes B and C that is in the swelled films (Table **3**). The conductivity of the swelled TBC2 film was in two orders higher than that of the dry film. An additional increase in the conductivity more than in order has been achieved in the swelled films contained the electrolyte. The best result was equal to $\sigma = 9.4\cdot10^{-3}$ S·cm^{-1}. Alteration in the electrolyte content in the films (Table **3**) did not practically influence their conductivity. Therefore, the following decrease in the electrolyte content in TBC2 films at the keeping high level of their ionic conductivity is possible.

In the other experimental series, we dealt with TBC3 films doped by lithium salt. The electrolyte content in the initial solution was varied relatively to TBC (Table **4**). In two cases, a nonionic plasticizer such as ethyleneglycol (EG) with the constant weight fraction (1 wt/% with respect to TBC) was also introduced (Table **4**). Significant increase in the film

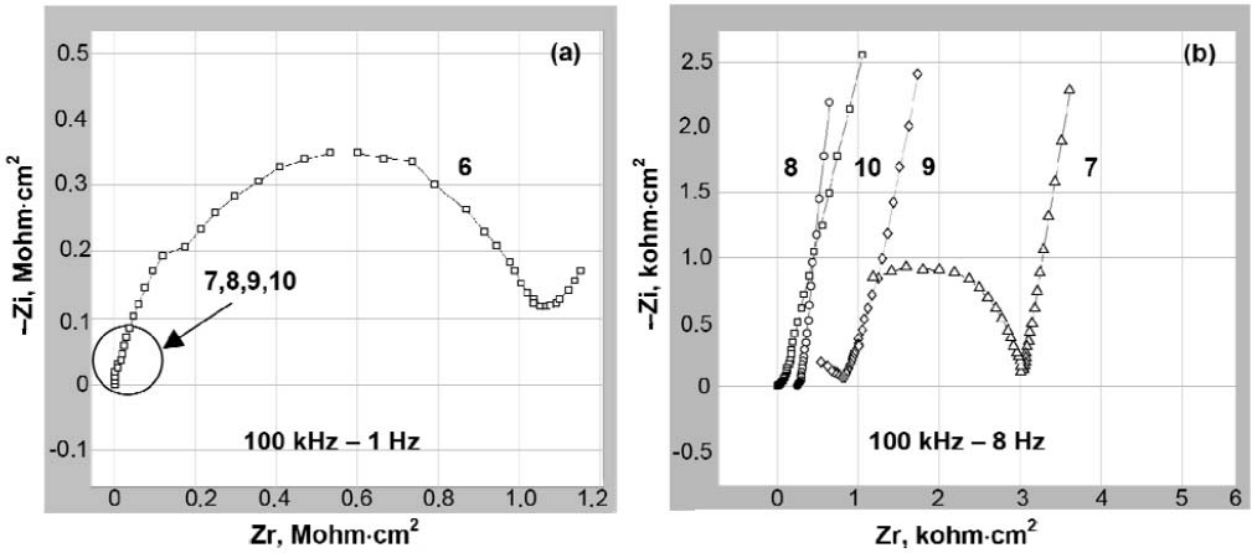

Figure 7: Impedance spectra for the compositions: TBC3+$LiPF_6$ and TBC3+$LiPF_6$+EG in different frequency regions; (**a**) film 6 in Table **4**, (**b**) films 7-10. The measurements were normalized for the cell area. The ratio of [EG]/[TBC] = 0.01 wt/wt was constant in all the systems.

Table 4: Ionic Conductivity of the Triblock Copolymer Doped by Lithium Salt

Film	System	[PEO]/[$LiPF_6$], base-mol·mol^{-1}	[TBC]/[$LiPF_6$], base-mol·mol^{-1}	l, μm	Processing procedure	σ, S·cm^{-1}
6	TBC3+$LiPF_6$	0.15	10.0	100	LE	$7.52\cdot10^{-6}$
7	TBC3+$LiPF_6$	0.09	5.7	125	ES	$1.43\cdot10^{-5}$
8	TBC3+$LiPF_6$	0.06	4.0	109	LE ES	$1.74\cdot10^{-5}$ $1.93\cdot10^{-5}$
9	TBC3+$LiPF_6$+EG	0.15	10.0	161	LE ES	$8.67\cdot10^{-6}$ $2.22\cdot10^{-5}$
10	TBC3+$LiPF_6$+EG	0.06	4.0	170	LE	$1.53\cdot10^{-4}$

elasticity took place at the addition of $LiPF_6$ and EG. The specific ionic conductivity of the compositions was also measured by impedance spectroscopy but only in the regime A. Frequency dependences of the imaginary and real parts of the complex impedance for TBC3 films doped by Li-salt are represented in Figure **7**. The volume resistances R_∞ of the films were determined from Figure **6** by means of two procedures: (LE) the linear extrapolation of experimental data to the abscissa-axis in the range of high frequencies and (ES) the extrapolation of the high-frequency semicircles, which were displayed in some impedance plots (Figure **7**), to the abscissa-axis [58,60].

All the results are represented in Table **4**. They showed a considerable rise in the ionic conductivity of the composite films with growth of $LiPF_6$ content.

Such effect was not surprising taking into account: i) corresponding increase in the concentration of ions in the films, and ii) the Li-ion interactions with oxygen atoms of PEO and/or carbonyls of PAAm amide groups [48]. The last interactions competed with hydrogen bonding of PEO and PAAm blocks and resulted in the plasticizing action of $LiPF_6$ additives on TBC3 film structure. A similar plasticizing action of Li-salts on the bulk structure of neat PEO and PEO-containing block copolymers is well known from the literature [28,30,58]. A small quantity of the nonionic plasticizer not only improved elasticity of the films but also essentially raised their conductivity. According to Table **4**, both the factors acted in the same direction. Thus, in TBC3 films doped by $LiPF_6$ together with EG, a high level of the ionic conductivity ($\sigma = 1.53\cdot10^{-4}$ S·cm^{-1} at 20 °C) has been achieved.

The value of σ is known to depend on too many factors: i) chemical nature, molecular parameters and structural organization of polymeric matrices, ii) chemical origin and concentration of electrolytes and other additives, and iii) the conditions of preparation and examination of polymer compositions. This does not allow carrying out the detailed comparison of σ values in different systems. At the same time, to show the level of the ionic conductivity of dry TBC films doped with Li-salt, we give below only some maximum σ values found in the following systems: i) the amorphous stochiometric InterPC(PMAAc+PEG) / $LiClO_4$ at a ratio of 8.1 base-$mol_{(PMAAc+PEG)}$/ mol_{LiClO4} ($\sigma = 1.2\cdot10^{-6}$ S·cm^{-1} at 25 °C) [39], ii) the composition (PEO+PAAc) / $LiClO_4$ at a ratio of 8 base-mol_{PEO} / mol_{LiClO4} ($\sigma = 6.3\cdot10^{-4}$ S·cm^{-1} at 20 °C) [40], iii) the amorphous dry layer-by-layer composition (PEO+PAAc) / $LiCF_3SO_3$ ($\sigma = 3.6\cdot10^{-10}$ S·cm^{-1} at 25 °C and the 1M Li-salt concentration in the initial PEO and PAAc solutions) [41], iv) the semi-crystalline PEO / $LiPF_6$ composition ($\sigma \approx 4.5\cdot10^{-5}$ S·cm^{-1} at 25 °C and Li-salt content of 20 w/%) [28], v) the partially crystalline cross-linked PEO / $LiClO_4$ ($\sigma \approx 1\cdot10^{-5}$ S·cm^{-1} at 30 °C) [34], vi) the partially crystalline multiblock copolymers $[PEO\text{-}b\text{-}PPO]_n$ included poly(propylene oxide) / $LiClO_4$ ($\sigma = 5.8\cdot10^{-4}$ at 25 °C and PPO content of 5 mol/% [62] and $\sigma = 4\cdot10^{-4}$ S·cm^{-1} at 30 °C and PPO fraction of 40 w/% [63]), vii) the partially crystalline multiblock copolymers $[PEO\text{-}b\text{-}PPO\text{-}b\text{-}PS]_n$ comprised polystyrene / $LiClO_4$ ($\sigma \sim 2\cdot10^{-4}$ S·cm^{-1} at 25 °C) [62], and finally viii) the multiblock copolymers $[PEO\text{-}b\text{-}PB\text{-}b\text{-}PS]_n$ contained polybutadiene / $LiClO_4$ ($\sigma \sim 1\cdot10^{-4}$ S·cm^{-1} at 35 °C) [64].

3. CONCLUSION

Experimental results and discussion above allow concluding that the following key structural factors ensured the high ionic conductivity of pure and doped TBC films could be picked out. The first important factor is the hydrogen bond system between PEO and PAAm blocks, due to which PEO chains lose their ability of crystallizing. The second one is a homogeneous distribution of the regions with

hydrogen-bonded segments of the components in the copolymer structure. Finally, the nanoporous mass-fractal organization of TBC structure takes also a significant role because it promotes a free and quick transport of low-molecular-weight electrolytes through the composite films under the action of external electric field.

ACKNOWLEDGEMENTS

The authors are grateful for the financial support provided by Kiev National Taras Shevchenko University. Additionally, this work was also partially supported by Ukrainian State Chemical-Engeneering University and Institute for Macromolecular Chemistry of National Academy of Sciences of Ukraine.

APPENDIX

TBC = triblock copolymer

PEO = poly(ethylene oxide)

AAm = acrylamide

PAAm = polyacrylamide

PAAc = poly(acrylic acid)

PMAAc = poly(methacrylic acid)

PS = polystyrene

PPO = poly(propylene oxide)

PB = polybutadiene

EG = ethylene glycol

DSSC = dye-sensitized solar cell

SSLB = solid-state lithium battery

InterPC = intermolecular polycomplex

IntraPC = intramolecular polycomplex

NMR = nucleic magnetic resonance

DSC = differential scanning carorimetry

FTIR = Fourier transform infrared spectroscopy

WAXS = wide-angle X-ray scattering

SAXS = small-angle X-ray scattering

DTGA = dynamic thermogravimetric analysis

LE = the linear extrapolation of impedance data to the abscissa-axis

ES = the extrapolation of high-frequency semicircles to the abscissa-axis

REFERENCES

[1] Vincent CA, Scrosati B. Modern batteries. An introduction to electrochemical power sources. 2nd ed. London: Arnold 1993.

[2] Lightfoot P, Metha MA, Brace PG. Structure of the polymer electrolyte poly(ethylene oxide) : $3LiCF_3SO_3$. Science 1993; 262: 883-5. http://dx.doi.org/10.1126/science.262.5135.883

[3] Gray FM. Polymer electrolytes. London: The Royal Society of chemistry monographs, Cambridge 1997.

[4] Nogueira AF, Durrant JR, De Paoli M-A. Dye-sensitized nanocrystalline solar cells employing a polymer electrolyte. Adv Mater 2001; 13: 826-30. http://dx.doi.org/10.1002/1521-4095(200106)13:11<826::AID-ADMA826>3.0.CO;2-L

[5] Stergiopoulos T, Arabatzis IM, Katsaros G, Falaras P. Binary polyethylene oxide/titania solid-state redox electrolyte for highly efficient nanocrystalline TiO_2 photoelectrochemical cells. Nano Lett 2002; 2: 1259-61. http://dx.doi.org/10.1021/nl025798u

[6] Kang MS, Kim JH, Kim YJ, Won J, Park N-G, Kang YS. Dye-sensitized solar cells based on composite solid polymer electrolytes. Chem Commun 2005; 889-91. http://dx.doi.org/10.1039/b412129p

[7] Stephan AM, Nahm KS. Review on composite polymer electrolytes for lithium batteries. Polymer 2006; 47: 5952-64. http://dx.doi.org/10.1016/j.polymer.2006.05.069

[8] Hagfeldt A, Boschloo G, Sun L, Kloo L, Pettersson H. Dye-sensitized solar cells. Chem Rev 2010; 110: 6595-63. http://dx.doi.org/10.1021/cr900356p

[9] Scrosati B, Garche J. Lithium batteries: status, prospects and future. J Power Sources 2010; 195: 2419-30. http://dx.doi.org/10.1016/j.jpowsour.2009.11.048

[10] Gupta RK, Rhee H-W. Highly conductive redox-couple solid polymer electrolyte system: blend-KI-I_2 for dye-sensitized solar cells. Adv OptoElectron 2011; 2011: ID 102932.

[11] Singh PK, Nagarale RK, Pandey SP, Rhee HW, Bhattacharya B. Present status of solid state photoelectrochemical solar cells and dye sensitized solar cells using PEO-based polymer electrolytes. Adv Nat Sci Nanosci Nanotechnol 2011; 2: 023002. http://dx.doi.org/10.1088/2043-6262/2/2/023002

[12] Kim YJ, Kim JH, Kang M-S, Lee MJ, Won J, Lee JC, *et al*. Supramolecular electrolytes for use in highly efficient dye-sensitized solar cells. Adv Mater 2004; 16: 1753-7. http://dx.doi.org/10.1002/adma.200306664

[13] Kim JH, Kang M-S, Kim YJ, Won J, Park N-G, Kang YS. Dye-sensitized nanocrystalline solar cells based on composite polymer electrolytes containing fumed silica nanoparticles. Chem Commun 2004; 1662-3. http://dx.doi.org/10.1039/b405215c

[14] Mohan VM, Murakami K. Dye sensitized solar cell with carbon doped (PAN/PEG) polymer quasi-solid gel electrolyte. J Adv Res Phys 2011; 2: 021112 (5pp).

[15] Appetecchi GB, Scaccia S, Passerini S. Investigation on the stability of the lithium polymer electrolyte interface. J Electrochem Soc 2000; 147: 4448-52. http://dx.doi.org/10.1149/1.1394084

[16] Appetecchi GB, Henderson W, Villano P, Berrettoni M, Passerini S. PEO-LiN($SO_2CF_2CF_3$)$_2$ polymer electrolytes. 1. XRD, DSC, and ionic conductivity characterization. J Electrochem Soc 2001; 148: A1171-8. http://dx.doi.org/10.1149/1.1403728

[17] Geiculescu OE, Yang J, Blau H, Bailey-Walsh R, Creager SE, Pennington WT, DesMarteau DD. Solid polymer electrolytes from dilithium salts based on new bis[(perf luoroalkyl)sulfonyl]diimide dianions. Preparation and electrical characterization. Solid State Ionics 2002; 148: 173-83. http://dx.doi.org/10.1016/S0167-2738(02)00111-X

[18] Kang M-S, Kim YJ, Won J, Kang YS. Roles of terminal groups of oligomer electrolytes in determining photovoltaic performances of dye-sensitized solar cells. Chem Commun 2005; 2686-8. http://dx.doi.org/10.1039/b418061e

[19] Rajendran S, Kannan R, Mahendran O. Ionic conductivity studies in poly(methylmethacrylate)-poly(ethylene oxyde) hybrid polymer electrolytes with lithium salts. J Power Sources 2001; 96: 406-10. http://dx.doi.org/10.1016/S0378-7753(00)00573-5

[20] Kim J, Park SJ, Kim S. Electrochemical properties of composite electrolytes based on poly(ethylene oxide)/poly(ethylene imine) containing the inorganic silica fillers. J Nanosci Nanotechnol 2012; 12: 685-9. http://dx.doi.org/10.1166/jnn.2012.5345

[21] Yang Y, Zhou C-H, Xu S, Hu H, Chen B-L, Zhang J, *et al*. Improved stability of quasi-solid-state dye-sensitized solar cell based on poly (ethylene oxide)–poly (vinylidene fluoride) polymer-blend electrolytes. J Power Sources 2008; 185: 1492-8. http://dx.doi.org/10.1016/j.jpowsour.2008.09.034

[22] Ahmad A, Rahman MYA, Suait MS. Morphological, infrared, and ionic conductivity studies of poly(ethylene oxide)-49% poly(methyl methacrylate) grafted natural rubber-lithium perchlorate salt based solid polymer electrolytes. J Appl Polym Sci 2012; 124: 4222-9. http://dx.doi.org/10.1002/app.35403

[23] Katsaros G, Stergiopoulos T, Arabatzis IM, Falaras P. A solvent-free composite polymer/inorganic oxide electrolyte for high efficiency solid-state dye-sensitized solar cells. J Photochem Photobiol A: Chem 2002; 149: 191-8. http://dx.doi.org/10.1016/S1010-6030(02)00027-8

[24] Zhang C, Wang M, Zhou X, Lin Y, Fang S, Li X, *et al*. Optimization of polymer electrolytes for quasi-solid state dye-sensitized solar cells. Chinese Sci Bull 2004; 49: 2033-6. http://dx.doi.org/10.1360/03wb0227

[25] Jung S, Kim DW, Lee SD, Cheong M, Nguyen DQ, Cho BW, *et al*. Fillers for Solid-State Polymer Electrolytes: Highlight. Bull Korean Chem Soc 2009; 30: 2355-61. http://dx.doi.org/10.5012/bkcs.2009.30.10.2355

[26] Zhang J, Huang X, Wei H, Fu J, Liu W, Tang X. Preparation and electrochemical behaviors of composite solid polymer electrolytes based on polyethylene oxide with active inorganic–organic hybrid polyphosphazene nanotubes as fillers. New J Chem 2011; 35: 614-21. http://dx.doi.org/10.1039/c0nj00717j

[27] Tang C, Hackenberg K, Fu Q, Ajayan PM, Ardebi H. High ion conducting polymer nanocomposite electrolytes using hybrid nanofillers. Nano Lett 2012; 12: 1152-6. http://dx.doi.org/10.1021/nl202692y

[28] Suriani I, Mohd RJ. Thermolysis and conductivity studies of poly(ethylene oxide) (PEO) based polymer electrolytes doped with carbon nanotubes. Int J Electrochem Sci 2012; 7: 2596-615.

[29] Bandara T, Dissanayake M, Ileperuma O, Varaprathan K, Vignarooban K, Mellander B-E. Polyethyleneoxide (PEO)-based, anion conducting solid polymer electrolyte for PEC solar cells. J Solid State Electrochem 2008; 12: 913-7. http://dx.doi.org/10.1007/s10008-007-0461-7

[30] Xie H-Q, Xie D. Molecular design, synthesis and properties of block and graft copolymers containing polyoxyethylene segments. Prog Polym Sci 1999; 24: 275-13. http://dx.doi.org/10.1016/S0079-6700(98)00020-3

[31] Zuo X, Liu X-M, Cai F, Yang H, Shen X-D, Li G. A novel all-solid electrolyte based on a co-polymer of poly-(methoxy/hexadecal-poly(ethylene glycol) methacrylate) for lithium-ion cell. J Mater Chem 2012; 22: 22265-71. http://dx.doi.org/10.1039/c2jm34270g

[32] Ghosh A, Kofinas P. PEO based block copolymer as solid state lithium battery electrolyte. ECS Transactions 2008; 11: 131-7. http://dx.doi.org/10.1149/1.2938916

[33] Niitani T, Shimada M, Kawamura K, Dokko K, Rho Y-H, Kanamura K. Synthesis of Li+ ion conductive PEO-PSt block copolymer electrolyte with microphase separation structure. Electrochem Solid-State Lett 2005; 8: A385-8. http://dx.doi.org/10.1149/1.1940491

[34] Ogata N. Ion-conducting polymers. J Macromol Sci Part C: Polym Rev 2002; C42: 399-39. http://dx.doi.org/10.1081/MC-120006454

[35] Uchiyama R, Kusagawa K, Hanai K, Imanishi N, Hirano A, Takeda Y. Development of dry polymer electrolyte based on polyethylene oxide with co-bridging agent crosslinked by electron beam. Solid State Ionics 2009; 180: 205-11. http://dx.doi.org/10.1016/j.ssi.2008.11.015

[36] Kang M-S, Kim JH, Won J, Kang YS. Dye-sensitized solar cells based on crosslinked poly(ethylene glycol) electrolytes. J Photochem Photobiol A: Chem 2006; 183: 15-21. http://dx.doi.org/10.1016/j.jphotochem.2006.02.013

[37] Xie H-Q, Zhou PG. Multicomponent polymer materials. In: Paul DR, Sperling CH, editors. Adv Chem Ser No 211. Washington DC: ACS 1986.

[38] Privalko VP, Novikov VV. The science of heterogeneous polymers. Structure and thermophysical properties. Chichester etc.: John Wiley & Sons 1995.

[39] Tsuchida E, Ohno H, Tsunemi K, Kobayashi N. Lithium ionic conduction in poly(methacrylic acid)-poly(ethylene oxide) complex containing lithium perchlorate. Solid State Ionics 1983; 11: 227-33. http://dx.doi.org/10.1016/0167-2738(83)90028-0

[40] An SY, Jeong IC, Won MS, Jeong ED, Shim Y-B. Effect of additives in PEO/PAA/PMAA composite solid polymer electrolytes on the ionic conductivity and Li ion battery performance. J Appl Electrochem 2009; 39: 1573-8. http://dx.doi.org/10.1007/s10800-009-9843-0

[41] DeLongchamp DM, Hammond PT. Highly ion conductive poly(ethylene oxide)-based solid polymer electrolytes from hydrogen bonding layer-by-layer assembly. Langmuir 2004; 20: 5403-11. http://dx.doi.org/10.1021/la049777m

[42] Jiang M, Li M, Xiang M, Zhou H. Interpolymer complexation and miscibility enhancement by hydrogen bonding. Adv Polym Sci 1999; 146: 121-96. http://dx.doi.org/10.1007/3-540-49424-3_3

[43] Dubin P, Bock J, Davis R, Schulz D, Thies C, Eds. Macromolecular complexes in chemistry and biology. Berlin-Heidelberg-New York: Springer-Verlag 1994. http://dx.doi.org/10.1007/978-3-642-78469-9

[44] Izumrudov VA, Zezin AB, Kabanov VA. Equilibria in interpolyelectrolyte reactions and the phenomenon of molecular "recognition" in solutions of interpolyelectrolyte complexes. Russ Chem Rev 1991; 60: 792-806. http://dx.doi.org/10.1070/RC1991v060n07ABEH001111

[45] Zheltonozhskaya T, Permyakova N, Momot L. Intramolecular polycomplexes in block and graft copolymers. In: Khutoryanskiy VV, Staikos G, editors. Hydrogen-bonded interpolymer complexes: formation, structure and applications. Ch. 5. New Jersey-London-Singapore etc.: World Scientific Publ. Corp 2009; pp. 85-154.

[46] Holappa S, Kantonen L, Winnik FM, Tenhu H. Self-complexation of poly(ethylene oxide)-*block*-poly(methacrylic acid) studied by fluorescence spectroscopy. Macromolecules 2004; 37: 7008-18. http://dx.doi.org/10.1021/ma049153n

[47] Fedorchuk SV, Zheltonozhskaya TB, Permyakova NM, Gomza YP, Nessin SD, Klepko VV. Structural peculiarities of triblock copolymers containing poly(ethylene oxide) and polyacrylamide. Mol Cryst Liq Cryst 2008; 497: 268-81. http://dx.doi.org/10.1080/15421400802463092

[48] Baron MH, Fillaux F. Vibrational spectra and structure of N-methylacetamide in some solid complexes with neutral salts. Can J Chem 1985; 63: 1473-6. http://dx.doi.org/10.1139/v85-252

[49] Lipatov YuS, Shilov VV, Gomza YuP, Kruglyak NE. X-Ray diffraction methods of analysis of polymer systems. Kyiv: Nauk. Dumka, UA 1982.

[50] Macdonald JR. Impedance spectroscopy. Ann Biomed Eng 1992; 20: 289-305. http://dx.doi.org/10.1007/BF02368532

[51] Permyakova NM, Zheltonozhskaya TB, Shilov VV, Zagdanskaya NE, Kunitskaya LR, Syromyatnikov VG, *et al*. Structure of triblock-copolymers based on poly(ethylene oxide) and poly(acrylamide) with central blocks of varying lengths. Theor Exper Chem 2005; 41: 382-8. http://dx.doi.org/10.1007/s11237-006-0007-6

[52] Privalko VP, Lobodina AP. Glass transition in the lower homologues of poly(ethylene oxide). Polym J 1974; 10: 1033-8.

[53] Feldstein MM. Peculiarities of glass transition temperature relation to the composition of poly(N-vinyl pyrrolidone) blends with short chain poly(ethylene glycol). Polymer 2001; 42: 7719-26. http://dx.doi.org/10.1016/S0032-3861(01)00225-7

[54] Shpak AP, Shilov VV, Shilova OA, Kunitskiy YuA. Diagnostics of nanosystems. Multilevel fractal structures (Part II). Kyiv: Nauk. Dumka, UA 2004.

[55] Zhang F, Ilavski J. Ultra-small-angle X-ray scattering of polymers. J Macromol Sci Part C: Polym Rev 2010; 50: 59-90.

[56] Beaucage G. Small-angle scattering from polymeric mass fractals of arbitrary mass-fractal dimension. J Appl Crystallography 1996; 29: 134-46. http://dx.doi.org/10.1107/S0021889895011605

[57] Barsoukov E, Macdonald JR. Impedance spectroscopy. Theory, experiment and applications. 2nd ed. New York: Wiley & Sons 2005. http://dx.doi.org/10.1002/0471716243

[58] Bruce PG, Ed. Solid State Electrochemistry. Cambridge: Cambridge Univ Press 1995.

[59] Sreekanth T, Jaipal Reddy M, Subba Rao UV. Polymer electrolyte system based on (PEO + $KBrO_3$) - its application as an electrochemical cell. J Power Sources 2001; 93: 268-72. http://dx.doi.org/10.1016/S0378-7753(00)00558-9

[60] Wang Y-P, Gao X-H, Li H-K, Li H-J, Liu H-G, Guo H-X. Effect of active filler addition on the ionic conductivity of PVDF-PEG polymer electrolyte. J Macromol Sci Part A: Pure Appl Chem 2009; 46: 461-7. http://dx.doi.org/10.1080/10601320902740277

[61] Singh PK, Kim KW, Kim KI, Park NG, Rhee HW. Nanocrystalline porous TiO_2 electrode with ionic liquid impregnated solid polymer electrolyte for dye sensitized solar cells. J Nanosci Nanotechnol 2008; 8: 5271-4. http://dx.doi.org/10.1166/jnn.2008.1069

[62] Xie H-Q, Liu ZS, Guo JS. Synthesis and properties of oxymethylene-linked oxyethylene-oxypropylene-styrene multiblock copolymers. Polymer 1994; 35: 4914-9. http://dx.doi.org/10.1016/0032-3861(94)90752-8

[63] Xie H-Q, Xie D, Chen X-Y, Guo J-S. Synthesis, characterization, and properties of two-component amphiphilic polyoxyethylene-containing multiblock copolymers. J Appl Polym Sci 2005; 95: 1295-301. http://dx.doi.org/10.1002/app.21012

[64] Xie H-Q, Tao XQ, Guo JS. Synthesis and properties of styrene–butadiene–oxyethylene multiblock polymers. J Appl Polym Sci 1996; 61: 407-13. http://dx.doi.org/10.1002/(SICI)1097-4628(19960718)61:3<407::AID-APP2>3.0.CO;2-M

Received on 03-09-2012 Accepted on 13-12-2012 Published on 31-12-2012

DOI: http://dx.doi.org/10.6000/1929-5995.2012.01.02.4